LA-UR-03-3113
Approved for public release;
distribution is unlimited.

May 13, 2003

Title: Pore Collapse and Hot Spots in HMX

Author(s): RALPH MENIKOFF

Submitted to: APS Topical Conference
Shock Compression of Condensed Matter
Portland, Oregon
July 20–25, 2003

PORE COLLAPSE AND HOT SPOTS IN HMX

Ralph Menikoff

Theoretical Division, MS-B214, Los Alamos National Laboratory, Los Alamos, NM 87545

Abstract. Hot spots are critical for initation of explosives because reaction rates are very temperature sensitive. For a plastic-bonded explosive, shock desensitization experiments imply that hot spots generated by pore collapse dominate shock initiation. Here, for the collapse of a single pore driven by a shock, the dependence of the temperature distribution on numerical resolution and dissipative mechanism is investigated. An inert material (with the constitutive properties of HMX) is used to better focus on the mechanics of pore collapse. Two important findings result from this study. First, insufficient resolution can significantly overpredict the hot-spot mass. Second, up to moderate piston velocities ($< 1\,$km/s), shock dissipation alone does not generate sufficient hot-spot mass for initiation. Two other dissipative mechanisms investigated are plastic work and viscous heating. In the cases studied, the integrated temperature distribution has a power-law tail with exponent related to a parameter with dimensions of viscosity. The parameter of either dissipative mechanism can be fit to obtain the hot-spot mass needed for initiation of any single experiment. However, the dissipative mechanisms scale differently with shock strength and pore size. Consequently, to predict initiation behavior over a range of stimuli and as the micro-structure properties of a PBX are varied, sufficient numerical resolution and the correct physical dissipative mechanism are essential.

INTRODUCTION

It has been known since the 1950s that initiation in a plastic-bonded explosive (PBX) is due to thermal reactions but requires hot spots [1]. Hot spots reconcile the large discrepancy between the time to detonation from Pop-plot data and the adiabatic induction time based on the bulk shock temperature and an Arrhenius reaction rate, see figure 1. For a strong shock ($P = 10\,$GPa) at the high end of the measured Pop plot in HMX-based PBX-9501, we note that the time to detonation is $\simeq 200\,$ns. Hot spots must react fast on this time scale, say within $20\,$ns, and would require a temperature of from $800\,$K based on the liquid phase reaction kinetics of Rogers [2] to $1500\,$K based on the "global reaction rate" of Henson *et al.* [3], see figure 2.

Shock desensitization experiments [4] and the increased sensitivity of a PBX with increasing porosity, as exhibited in Pop-plot data, imply that hot spots generated by pore collapse dominate a shock-to-detonation transition. Early hydrodynamic simulations of heterogeneous initiation by Mader [5, sec. 3.3] utilized artificial viscosity for shock waves as the only dissipative mechanism. They showed that, when a strong shock impinges on a pore, a micro-jet is formed and subsequently produces a hot spot on impact with the downstream side of the pore. Furthermore, Mader's simulations with arrays of pores in an explosive showed a shock-to-detonation transition. When the simulations were performed (2-D flow in the 1960s and 3-D in the 1980s), the available computer power limited the resolution. In addition, the equation of state for the explosive had a constant specific heat. The specific heat for HMX varies by a factor of 2 between room temperature and $1000\,$K, and can have a large effect on the reaction rate because of its sensitivity to temperture.

With only shock dissipation, the peak pore collapse temperature can be estimated based solely on the equation of state (EOS) of the explosive and simple Riemann problems. For β-HMX a complete EOS

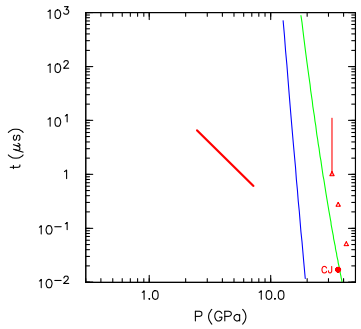

FIGURE 1. Time to detonation as function of shock pressure for HMX. Red line is Pop plot for PBX-9501 [6]. Blue and green lines are adiabatic induction time for Arrhenius reaction rate based on liquid HMX [2] and "global reaction rate" [3], respectively. Symbols are from wedge experiments of single crystal HMX by Craig [4].

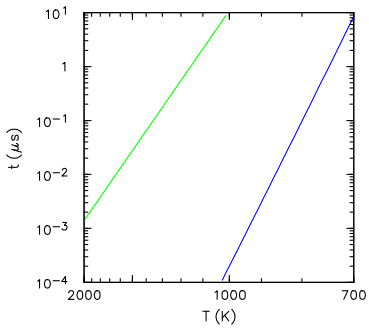

FIGURE 2. Adiabatic induction time for HMX. Blue and green lines are based on Arrhenius reaction rate for liquid HMX [2] and "global reaction rate" [3], respectively.

derived from data currently available and estimates of the hot-spot temperature have been presented [7]. Since the EOS neglects the β-liquid phase transition, which has a latent heat equivalent to $\Delta T \simeq 200\,\mathrm{K}$, we take $T = 1000\,\mathrm{K}$ as the critical hot-spot temperature for fast reaction. The estimates in [7] indicate that shock dissipation alone does not generate sufficiently high hot-spot temperatures, even for a strong shock at the high end of the measured Pop plot.

Other dissipative mechanisms applicable to pore collapse are viscous heating and plastic work. In the past, hot-spot temperatures were estimated based on simplified models due to the limited computer power available at the time; see for example [8, 9]. Here, for the collapse of a single pore driven by a shock, the dependence of the temperature distribution on numerical resolution and dissipative mechanism is investigated.

We consider both shear viscosity and rate-dependent plasticity. These dissipative mechanisms introduce a parameter η with dimensions of dynamic viscosity. For plasticity, the parameter determines the relaxation rate to the yield surface. The viscous parameter gives rise to two dimensionless parameters: Reynolds number, $Ry = \frac{\rho u R}{\eta}$ and (shock width)/(pore radius). Consequently, scaling of hot-spot temperature with pore radius and particle velocity will depend on the dissipative mechanism. To study this dependence we choose to hold the pore radius fixed and vary the viscosity parameter.

SIMULATIONS

Initial conditions for two-dimensional simulations are a gas-filled pore of radius 0.1 mm centered at (0.4,0.0) mm and surrounded by an inert material at 300 K with the EOS properties of HMX. A piston at the left boundary with a velocity of 1.3 km/s is used to drive a shock wave with a pressure of 13 GPa and temperature of 630 K.

For hydrodynamic pore collapse, in which the only dissipation is at shock fronts, figure 3A shows the temperature field after the shock front has passed over the pore. Pore collapse gives rise to an outgoing rarefaction wave in the material compressed by the lead shock, followed by an outgoing shock wave. These secondary waves give rise to the main features seen in the temperature field. We note that the secondary shock has caught up to the lead shock, resulting in a Mach wave pattern. The temperature discontinuity corresponds to the contact emanating from the Mach triple point at (0.82,0.14). The gas pore has been highly compressed and distorted by the vortex set up from the impact of the micro-jet, formed when the lead shock overtakes the pore, on the downstream side of the pore. Since the vortex and the gas interface are expected to be unstable, the shape of the pore is presumably inaccurate in detail.

The temperature distribution is shown in figure 3B. The first peak at 300 K corresponds to the ambient state ahead of the lead shock front. The second peak centered at 575 K corresponds to the material heated by the lead shock and then cooled by the rarefaction from the pore implosion. The third

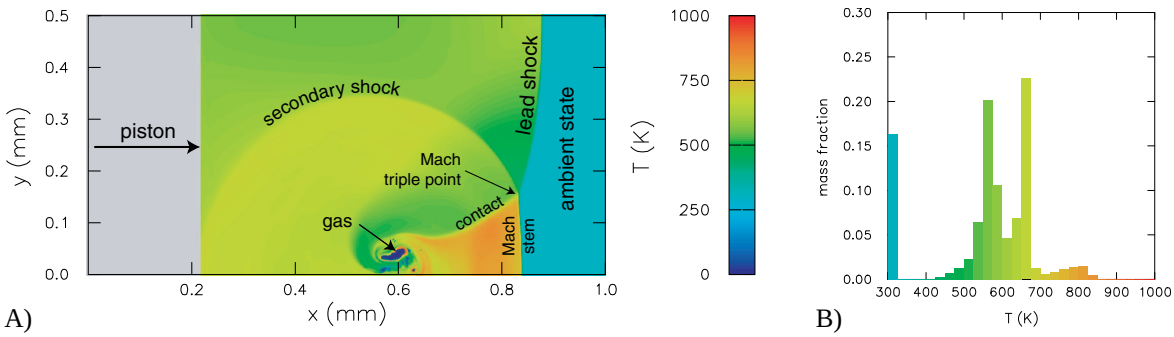

FIGURE 3. Temperature after pore collapse. Simulation with piston velocity of 1.3 km/s, shock dissipation only, and resolution of 100 cells in the initial pore radius (0.1 mm). A) 2-D temperature field. Bottom boundary is symmetry plane. B) Temperature distribution.

peak centered about 675 K corresponds to the material heated by the lead shock and backward expanding portion of the secondary shock from the explosion of the pore. The low broad peak between 700 and 850 K corresponds to the region between the Mach stem and the material directly impacted by the micro-jet. The highest HMX temperatures, above 850 K, occur only near the pore and are numerical artifacts of the material interface treatment. The peak temperature is consistent with the estimates based on Riemann problems [7].

We note that the third peak is similar to what Hayes [10, Fig. 5] used to model initiation in HNS. The temperature of this peak depends on the explosive through its equation of state and specific heat. Since 1000 K is needed for fast reactions in HMX, we conclude that shock dissipation alone is not sufficient for initiation.

With additional dissipative mechanisms, *e.g.* plastic work or viscous heating, the tail of the temperature distribution can be greatly enhanced. Consequently, the reaction from hot spots is associated with the extreme tail of the temperature distribution. The tail of the temperature distribution is best described by the integrated temperature distribution, mass(T_1) at $T_1 > T$. It is convenient to normalize the mass relative to the equivalent mass in the pore volume at the initial explosive density.

We next examine the effect of mesh resolution on the temperature distribution. Figure 4 shows the integrated temperature distribution, with shock dissipation only, as the resolution is varied from 5 to 100 cells in the initial pore radius. We note that the distributions are nearly the same up to 800 K, but differ substantially in the high temperature tail. The differences are largely due to truncation errors from discretizing the flow equations in the underresolved region of high vorticity around the pore.

The low resolution case has sufficient hot-spot mass above 1000 K that, if the simulation included chemical reaction, a substantial amount of burn would occur — roughly a burn mass equivalent to 25% of the volume of the pore. Thus, errors from too low a resolution can substantially affect simulations of initiation. This is an important concern for mesoscale simulations of hot-spot initiation, and is a determining factor in the size or number of grains in a PBX that can be included in the computational domain.

Simulations with additional dissipative mechanisms are summarized by the integrated temperature distribution shown in figure 5. We observe that the tail of the distributions, above 700 K, are approximately linear on a log-log scale. This implies that the tail of the distribution can be approximated with a power-law. Moreover, the exponent of the power-law is related to the viscous parameter such that the effective hot-spot mass increases as the viscous parameter increases.

The viscous parameter has not been directly measured. Instead, it is usually fit to reproduce integral data from a limited class of experiments. The fact that both the viscous heating and plastic work have similar distributions implies that either dissipative mechanism can be used in a fit. To discriminate between these mechanism requires a range of experiments that are sensitive to differences in the scaling behavior of each mechanism.

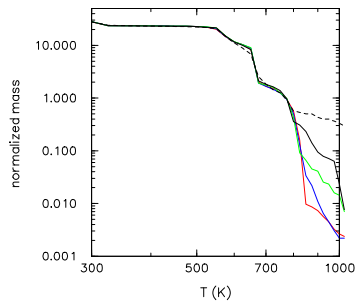

FIGURE 4. Variation of temperature distribution with resolution for shock dissipation only. Cells in pore radius: red, 100; blue, 50; green, 20; black, solid and dashed, 10 and 5, respectively.

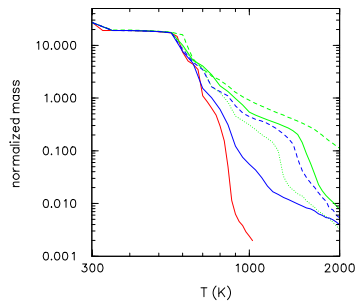

FIGURE 5. Variation of temperature distribution with dissipative mechanism. Dissipative mechanisms: red, shock heating; blue, shear viscosity, solid and dashed $\eta =$ 10 and 100 Poise, respectively; green, rate-dependent plasticity, solid, dashed and dotted $\eta = 800$, 8000 and 80 Poise, respectively.

CONCLUSIONS

Two important findings resulted from this study. First, too low a resolution can significantly enhance the hot-spot mass. Second, up to modest piston velocities (< 1 km/s), shock dissipation alone does not generate sufficient hot-spot mass. Two other dissipative mechanisms investigated are plastic work and viscous heating. In the cases studied, the integrated temperature distribution has a power-law tail with exponent related to a parameter with dimensions of viscosity. The dissipative mechanisms scale differently with shock strength and pore size. Consequently, to predict initiation behavior over a range of stimuli and as the microstructural properties of a PBX are varied, sufficient numerical resolution and the correct physical dissipative mechanism are essential.

ACKNOWLEDGMENTS

This work was carried out under the auspices of the U. S. Dept. of Energy at LANL under contract W-7405-ENG-36. The author thanks Prof. David Benson, Univ. of Calif. at San Diego, for providing the code used for the simulations.

REFERENCES

1. Bowden, F. P., and Yoffe, Y. D., *Initiation and Growth of Explosion in Liquids and Solids*, Cambridge Univ. Press, Cambridge, UK, 1952.
2. Rogers, R. N., *Thermochimica Acta*, **11**, 131–139 (1975).
3. Henson, B. F., Asay, B. W., Smilowitz, L. B., and Dickson, P. M., Ignition chemistry in HMX from thermal explosion to detonation, Tech. Rep. LA-UR-01-3499, Los Alamos National Lab. (2001).
4. Campbell, A. W., and Travis, J. R., "The Shock Desensitization of PBX-9404 and Composition B-3," in *Eighth Symposium (International) on Detonatione*, 1985, pp. 1057–1068.
5. Mader, C. L., *Numerical Modeling of Explosives and Propellants*, CRC Press, Baca Raton, FL, 1998, second edn.
6. Gibbs, T. R., and Popalato, A., editors, *LASL Explosive Property Data*, University of California Press, 1980.
7. Sewell, T. D., and Menikoff, R., "Complete Equation of State for β-HMX and Implications for Initiation," in *Shock Compression of Condensed Matter*, 2003, this volume.
8. Khasainov, B. A., Attetkov, A. V., Borisov, A. A., Ermolaev, B. S., and Soloviev, V. S., "Critical Conditions for Hot Spot Evolution in Porous Explosives," in *Progress in Astronautics and Aeronautics*, 1988, vol. 114, pp. 303–321.
9. Frey, R. B., "Cavity Collapse in Energetic Materials," in *Eighth Symposium (International) on Detonation*, 1985, pp. 68–80.
10. Hayes, D. B., "Shock Induced Hot-Spot Formation and Subsequent Decomposition in Granular, Porous HNS Explosive," in *Progress in Astronautics and Aeronautics*, 1983, vol. 87, pp. 445–467.